

Study of forbidden atomic transitions on D_2 line using Rb nano-cell placed in external magnetic field

G. Hakhumyan^{1,2}, C. Leroy², R. Mirzoyan^{1,2}, Y. Pashayan-Leroy², and D. Sarkisyan¹

¹ Institute for Physical Research, NAS of Armenia, Ashtarak 0203, Armenia

² Laboratoire Interdisciplinaire Carnot de Bourgogne, UMR CNRS 5209, Université de Bourgogne, 21078 Dijon Cedex, France

Received: date / Revised version: date

Abstract. By experimental exploration of the so-called λ -Zeeman technique based on Rb nano-cell use we reveal for the first time a strong modification of the probability of the ^{87}Rb , D_2 line $F_g = 1 \rightarrow F_e = 0, 1, 2, 3$ atomic transitions, including forbidden $F_g = 1, m_F = 0 \rightarrow F_e = 1, m_F = 0$ and $F_g = 1, m_F = -1 \rightarrow F_e = 3, m_F = -1$ transitions (these are forbidden transitions when $B = 0$) in a strong external magnetic field B in the range of 100 – 1100 G. For π -polarized exciting diode laser radiation ($\lambda = 780$ nm) these forbidden transitions at $B > 150$ G are among the strongest atomic transitions in the detected transmission spectra. Frequency shifts of the individual hyperfine transitions versus magnetic field are also presented: particularly, $F_g = 1, m_F = +1 \rightarrow F_e = 1, m_F = +1$ atomic transition has a unique behavior, since its frequency remains practically unchanged when B varies from 100 to 1100 G. Developed theoretical model well describes the experiment.

1 Introduction

Alkali atoms, particularly Rb atoms, are widely used in laser atomic physics due to strong atomic transitions with the wavelength located in the near infrared region. It is also important that there are available diode lasers with good parameters which wavelength is resonant with the atomic transitions. Rb atoms are widely used in laser cooling experiments, information storage, spectroscopy, magnetometry *etc* [1,2]. Of a special interest are the ^{87}Rb atoms used in Bose-Einstein Condensates (BEC) experiments [1]. That's why a detailed knowledge of the behavior of Rb atomic transitions, particularly, in an external magnetic field is of high importance. It is well-known that atomic energy levels split in a magnetic field into Zeeman sub-levels, and frequency shifts of atomic transitions between ground and

upper sub-levels (optical domain) deviate from the linear behavior in quite moderate magnetic field [3,4]. Also, atomic transition probabilities undergo significant changes depending on external magnetic B -field [3]. Usually, frequency separation between atomic transitions in an external magnetic field of 50 – 1000 G achieves 20 – 200 MHz. However, because of Doppler broadening (~ 500 MHz), in order to study separately each individual atomic transition behavior one should implement a technique providing sub-Doppler resolution.

It is known that, with the saturated absorption (SA) technique, the sub-Doppler spectral resolution can be achieved using conventional centimeter-scale cells. In Refs. [5,6] the SA technique is used to study spectra of D_2 line of Rb atoms. However, one of the significant disadvantages of the SA technique is the presence of the so-called cross-over resonances in the spectra. In a magnetic field, these resonances split into numerous components, making the spectrum very difficult to analyze. This restricts the magnitude of acceptable magnetic field below 100 G. Another disadvantage of the SA technique is the fact that, the amplitudes of velocity selective optical pumping (VSOP) resonances formed in SA spectrum do not correspond to the probabilities of the corresponding atomic transitions. This additionally strongly complicates the analysis of spectra. Note, that sub-Doppler spectral resolution could be obtained by using expensive and complicated systems based either on cold and trapped atoms or with the help of collimated several-meter long Rb atomic beam propagated in vacuum conditions.

Recently, it has been demonstrated that a one-dimensional nano-metric thin cell (NTC) filled with Rb atoms is a very convenient tool to obtain sub-Doppler spectral resolution when the thickness L of atomic vapor column is either $L = \lambda/2$ or $L = \lambda$, where λ is the laser radiation wavelength resonant with the Rb D_1 or D_2 lines ($\lambda = 794$ nm or 780 nm). In case of the thickness $L = \lambda/2$ it is more convenient to use the fluorescence of the NTC since the spectrum linewidth is 7 – 8 times narrower than that of the Doppler width obtained with a conventional cm-size Rb cell. The method is called "half- λ Zeeman technique" (HLZT) [7,8,9].

In case of the thickness $L = \lambda$ spectrally-narrow VSOP resonances appear at laser intensities ~ 10 mW/cm² in the transmission spectrum of NTC. The formation of VSOP resonances with the help of NTC has several advantages in comparison with the SA technique: i) the absence of cross-over resonances, which is very important for some applications, particularly, when an external magnetic field is applied; ii) the ratio of amplitudes of VSOP resonances is close to the ratio of the corresponding atomic transition probabilities; iii) a single beam transmission is used; iv) the laser power required for the formation of VSOP resonances is as low as 0.1 mW. In a magnetic field these VSOP resonances are split into several new components, the number of which depends on the quantum numbers F of the lower and upper levels, while the amplitudes and frequency positions of the components depend on B -field. This method allows one to study separately each individual atomic transition behavior (" λ -Zeeman technique" (LZT)) [10,11,12,13].

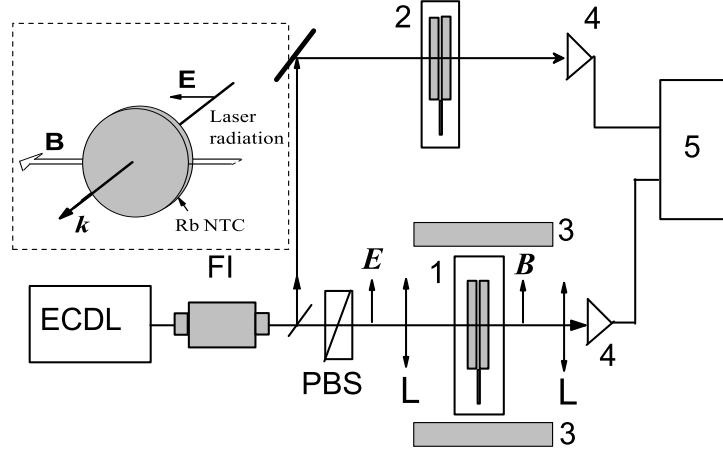


Fig. 1. Sketch of the experimental setup. *ECDL* - diode laser, *FI* - Faraday isolator, *1* - NTC in the oven, *2* - an auxiliary NTC and the oven, *PBS* - polarization beam splitter, *3* - permanent magnets (PMs), *L* - lenses, *4* - photodetectors, *5* - digital storage oscilloscope, \mathbf{E} - electrical field of laser radiation, \mathbf{B} - magnetic field applied to NTC, \mathbf{B}/\mathbf{E} . Configuration of the magnetic measurement is presented in the inset in the dashed square.

Below are presented the results of the experimental study of the ^{87}Rb , D_2 line $F_g = 1 \rightarrow F_e = 0, 1, 2, 3$ atomic transitions, including forbidden $F_g = 1, m_F = 0 \rightarrow F_e = 1, m_F = 0$ and $F_g = 1, m_F = -1 \rightarrow F_e = 3, m_F = -1$ transitions for π -polarized exciting laser radiation. For this study Rb NTC is placed in a strong external magnetic field B varying in the range of 100 – 1100 G. A theoretical model applied to describe the experimental results is presented.

2 Experiment

2.1 Experimental setup

The first design of the NTC (also called extremely thin cell) consisting of windows and a vertical side arm (a metal reservoir), is presented in [14]. Later, this design has been somehow modified and a typical example of a recent version is given in [9]. The used NTC has garnet windows of 2.4 mm thickness. The NTC is filled with a natural mixture of ^{85}Rb (72.2%) and ^{87}Rb (27.8%). Our study concerns the region of $L \approx \lambda \approx 780$ nm. The temperature limit of the NTC operation is 400 °C. The NTC operated with a specially designed oven (made from non-magnetic materials) with two ports for laser beam transmission. The source temperature of the atoms of the NTC was 120 °C, corresponding to the vapor density $N = 2 \times 10^{13} \text{ cm}^{-3}$, but the windows were maintained at a temperature that was 20 °C higher.

The sketch of the experimental setup is shown in Fig. 1. The π -polarized beam of extended cavity diode laser (ECDL, $\lambda = 780$ nm, $P_L = 30$ mW, $\gamma_L < 1$ MHz) resonant with the ^{87}Rb , D_2 transition frequency, is focused (the laser spot diameter is ≤ 0.1 mm) at nearly normal incidence onto the Rb NTC 1 with the vapor column thickness $L = \lambda = 780$ nm. To avoid feedback a Faraday insulator is applied. A polarization beam splitter PBS is used to purify initial linear radiation polarization of the laser. A part of the pumping radiation was directed to the auxiliary (reference) Rb NTC 2, which was in zero magnetic field; transmission spectrum of this NTC is used as a frequency reference. The transmission signal was detected by a photodiode 4 and was recorded by Tektronix TDS 2014 B digital four-channel storage oscilloscope 5. Moderate magnetic fields in the range of 10 – 200 G are produced by Helmholtz coils, while in order to produce strong magnetic fields ($B > 200$ G) two strong permanent magnets (PMs) 3 are used [11]. In both cases \mathbf{B} is directed along the laser electric field direction \mathbf{E} ($\mathbf{B} // \mathbf{E}$). The configuration of the magnetic measurement is presented in the inset in Fig. 1. The B -field strength was measured by a calibrated Hall gauge.

2.2 Experimental results and discussion

The atomic transitions $F_g = 1 \rightarrow F_e = 0, 1, 2, 3$ between magnetic sub-levels of hyperfine states for the ^{87}Rb , D_2 line (optical domain) in the case of π -polarized laser radiation excitation are depicted in Fig. 2. Note that when $B = 0$ according to the selection rules the atomic transitions with the corresponding $\Delta F = 2$, namely $F_g = 1 \rightarrow F_e = 3$ and $F_g = 1, m_F = 0 \rightarrow F_e = 1, m_F = 0$ transitions are strongly forbidden, while all other presented transitions with $\Delta F = F_g - F_e = 0, \pm 1$ and $\Delta m_F = 0$ are allowed [15].

As it was recently shown, λ -Zeeman technique implemented in case of σ^+ (left circular) polarized excitation allows one to study separately each individual atomic transition behavior in an external magnetic field [10,11]. As demonstrated below, the λ -Zeeman technique implemented in case of π -polarized excitation is also very convenient, since the examination of the VSOP resonances formed in the NTC allows one to obtain, identify, and investigate each individual atomic transition between the Zeeman sub-levels in the transmission spectrum of the ^{87}Rb D_2 line in a very wide range of magnetic fields from a few tens up to several thousands of Gauss.

The two upper curves in Fig. 3 show the transmission spectra from the Rb nano-cell $L = \lambda = 780$ nm for the magnetic field $B \approx 147$ G and 167 G, with π -polarized exciting laser radiation (VSOPs numbers denote the corresponding transitions depicted in Fig. 2). The magnetic field is produced by Helmholtz coils (the maximum available B -field is ~ 200 G). The splitting and shifts of the three VSOP resonances 2, 5, and 8 are clearly seen in Fig. 3. Thus, the remarkable result is that the forbidden transition $F_g = 1, m_F = 0 \rightarrow F_e = 1, m_F = 0$ labeled 5 at $B \sim 150$ G is among the three strongest atomic transitions, while the other transitions have smaller probabilities,

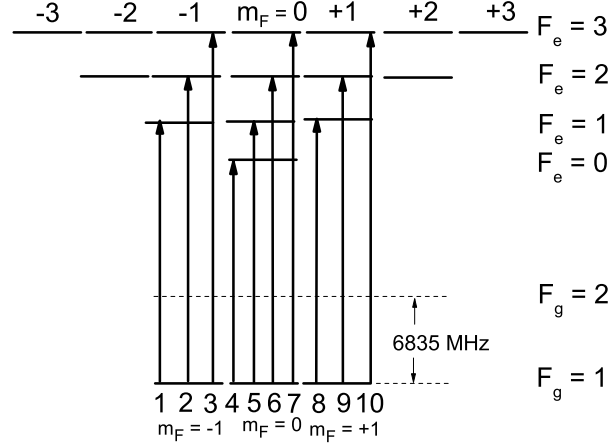


Fig. 2. Energy levels diagram of the D_2 line of ^{87}Rb and $F_g = 1 \rightarrow F_e = 3$ atomic transitions for π -polarized exciting laser radiation ($\Delta m_F = 0$)

and thus are not detectable in the spectra (this is confirmed by the theory - see below). The lower grey curve is the transmission spectrum as given by the reference nano-cell which shows the positions of the atomic transitions, i.e., the VSOP resonances (with the linewidth of ~ 20 MHz) for $B \sim 0$. We measure the atomic frequency shifts with respect to the initial position of $F_g = 1 \rightarrow F_e = 1, 2, 3$ transition in the studied nano-cell in the magnetic field \mathbf{B} directed along the laser radiation electric field \mathbf{E} .

Figure 4 demonstrates the transmission spectra for the atomic transitions $F_g = 1 \rightarrow F_e = 0, 1, 2, 3$ at the following values of the magnetic field B : 231, 275 and 316 G. As mentioned, a strong magnetic field is produced by two PMs (with the diameter of 60 mm) placed on the opposite sides of the nano-cell oven and separated by a variable distance. To control the magnetic field value, one of the magnets is mounted on a micrometric translation stage for longitudinal displacement. The splitting and shifts of the six VSOP resonances 2, 5, 8, 3, 6 and 9 are clearly seen. Note, that at $B \geq 230$ G the forbidden transition labeled 5 together with another forbidden transition $F_g = 1, m_F = -1 \rightarrow F_e = 3, m_F = -1$ labeled 3 is among the four strongest atomic transitions (this is also confirmed by the theory - see below).

Figure 5 shows transmission spectra for the atomic transitions for the following values of the magnetic fields, $B_{1,2,3,4,5} = 700, 740, 865, 1010$ and 1080 G, correspondingly. Again, the splitting and shifts of the six VSOP resonances 2, 5, 8, 3, 6 and 9 are clearly seen. Importantly, the both forbidden transitions labeled 3 and 5 are always among the four strongest atomic transitions. Note, that at $B \geq 700$ G the ^{85}Rb , D_2 line, $F_g = 2 \rightarrow F_g = 1, 2, 3$ atomic transitions (marked by the vertical arrows) are also detected. However, up to ~ 1100 G the influence of the ^{85}Rb , D_2 line atomic

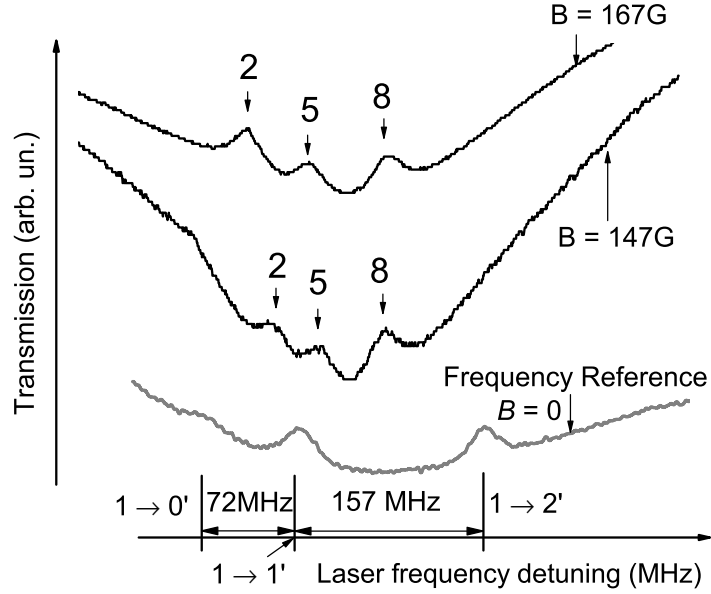


Fig. 3. Transmission spectra from the Rb NTC ($L = \lambda = 780$ nm) for transitions $F_g = 1 \rightarrow F_e = 0, 1, 2, 3$ vs magnetic field. VSOPs numbers denote the corresponding transitions depicted in Fig. 2. Forbidden transition $F_g = 1, m_F = 0 \rightarrow F_e = 1, m_F = 0$ labeled 5 at $B \sim 150$ G is among the three strongest atomic transitions. The lower grey curve is the transmission spectrum from the reference Rb NTC ($L = \lambda$). The spectra are shifted vertically for convenience.

transitions doesn't affect strongly the ^{87}Rb spectra. A striking point is also as follows: the variation of the magnetic field in the range of 100 – 1100 G practically doesn't cause frequency shift of unique $F_g = 1, m_F = +1 \rightarrow F_e = 1, m_F = +1$ atomic transition labeled 8 (this is also confirmed by the theory - see here after).

3 Theoretical model and discussions

In this work the main interest is to study the behavior of the ^{87}Rb , $F_g = 1 \rightarrow F_e = 0, 1, 2, 3$ transitions, D_2 line in the case of π -excitation. Theoretical model describes how to provide the calculations of separated transitions' frequencies and amplitude modification undergo external magnetic field (the details of the theory are presented in [3,16]). We adopt a matrix representation in the coupled basis, that is, the basis of the unperturbed atomic state vectors $|(n=5), L, J, F, m_F\rangle$ to evaluate the matrix elements of the Hamiltonian describing our system. In this basis, the diagonal matrix elements are given by

$$\langle F, m_F | H | F, m_F \rangle = E_0(F) + \mu_B g_F m_F B, \quad (1)$$

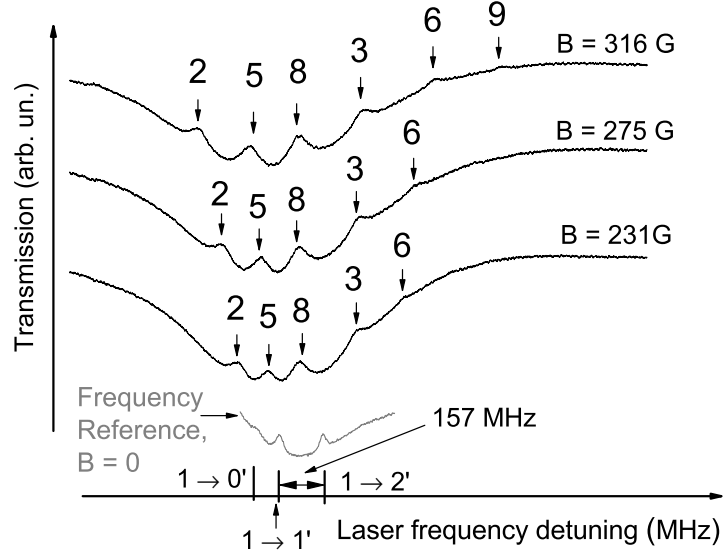


Fig. 4. Transmission spectra from the Rb NTC $L = \lambda = 780$ nm for atomic transitions $F_g = 1 \rightarrow F_e = 0, 1, 2, 3$ versus magnetic field B : 231, 275 and 316 G. Numbers denote the corresponding transitions depicted in Fig. 2. Forbidden transition $F_g = 1, m_F = -1 \rightarrow F_e = 3, m_F = -1$ labeled 3 at $B \geq 230$ G is among the four strongest atomic transitions. The lower grey curve is the transmission spectrum from the reference Rb NTC $L = \lambda = 780$ nm.

where $E_0(F)$ is the initial energy of the sub-level $|(n=5), L, J, F, m_F\rangle \equiv |F, m_F\rangle$ and g_F is the effective Landé factor.

The off-diagonal matrix elements are non-zero for levels verifying the selection rules $\Delta L = 0, \Delta J = 0, \Delta F = \pm 1, \Delta m_F = 0$,

$$\begin{aligned} \langle F-1, m_F | H | F, m_F \rangle &= \langle F, m_F | H | F-1, m_F \rangle = -\frac{\mu_B B}{2} (g_J - g_I) \\ &\times \left(\frac{[(J+I+1)^2 - F^2][F^2 - (J-I)^2]}{F} \right)^{1/2} \left(\frac{F^2 - m_F^2}{F(2F+1)(2F-1)} \right)^{1/2}. \end{aligned} \quad (2)$$

The diagonalization of the Hamiltonian matrix allows one to find the eigenvectors and the eigenvalues, that is to determine the eigenvalues corresponding to the energies of Zeeman sub-levels and the new states vectors which can be expressed in terms of the initial unperturbed atomic state vectors,

$$|\Psi(F_e, m_e)\rangle = \sum_{F'_e} \alpha_{F_e F'_e}^e(B) |F'_e, m_e\rangle \quad (3)$$

and

$$|\Psi(F_g, m_g)\rangle = \sum_{F'_g} \alpha_{F_g F'_g}^g(B) |F'_g, m_g\rangle. \quad (4)$$

The state vectors $|F'_e, m_e\rangle$ and $|F'_g, m_g\rangle$ are the unperturbed state vectors, respectively, for the excited and the ground states. The coefficients $\alpha_{F_e F'_e}^e(B)$ and $\alpha_{F_g F'_g}^g(B)$ are mixing coefficients, respectively, for the excited and the

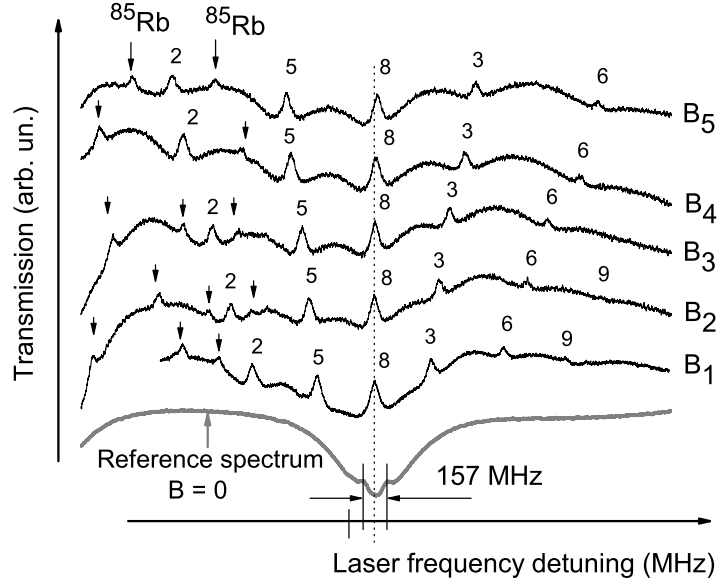


Fig. 5. Transmission spectra from the Rb NTC $L = 780$ nm for atomic transitions $F_g = 1 \rightarrow F_e = 0, 1, 2, 3$ versus magnetic field $B_{1,2,3,4,5} = 700, 740, 865, 1010$ and 1080 G, correspondingly. Numbers denote the corresponding transitions depicted in Fig. 2. Forbidden transitions 5 and 3 at $B \geq 700$ G are among the four strongest atomic transitions. The atomic transition labeled 8 is a unique one since its frequency remains practically unchanged (vertical dotted line is presented for the eye-guide) when B varying in the range of $100 - 1100$ G. The lower grey curve is the reference one.

ground states; they depend on the field strength and magnetic quantum numbers m_g or m_e . Diagonalization of the Hamiltonian matrix for ^{87}Rb , D_2 line, in case of π -polarization of exciting radiation, allows obtaining the shift of position of energy levels in presence of external magnetic field.

The probability of a transition, induced by the interaction of the atomic electric dipole and the oscillating laser electric field is proportional to the spontaneous emission rate of the associated transition A_{eg} , that is, to the square of the transfer coefficients modified by the presence of the magnetic field

$$W_{eg} \propto A_{eg} \propto a^2 [\Psi(F_e, m_e); \Psi(F_g, m_g); q], \quad (5)$$

The transfer coefficients are expressed as

$$a [\Psi(F_e, m_e); \Psi(F_g, m_g); q] = \sum_{F'_e F'_g} \alpha_{F_e F'_e}^e(B) a(\Psi(F_e, m_e); \Psi(F_g, m_g); q) \alpha_{F_g F'_g}^g(B), \quad (6)$$

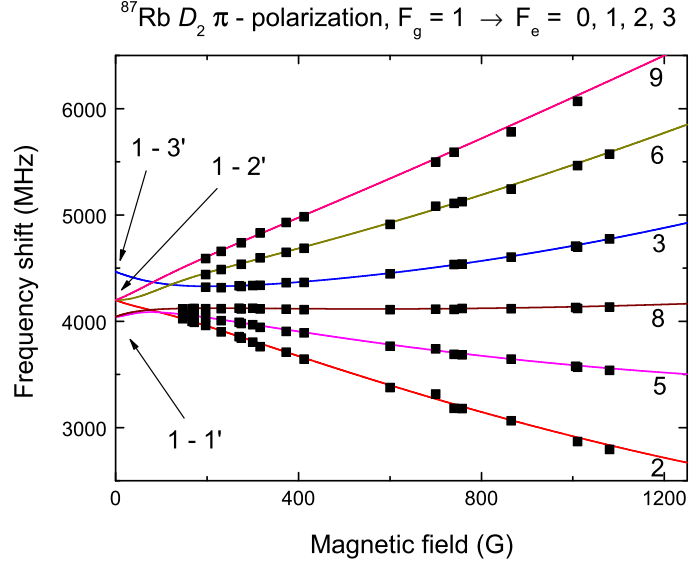


Fig. 6. Frequency shift of components 2, 5, 8, 3, 6 and 9 versus B -field relative to the initial position (indicated by the arrows at $B = 0$), the black squares are the experimental results and the solid curves are the calculated ones (numbers denote the corresponding transitions, see Fig. 2)

where the unperturbed transfer coefficients have the following definition

$$a(\Psi(F_e, m_e); \Psi(F_g, m_g); q) = (-1)^{1+I+J_e+F_e+F_g-m_e} \times \sqrt{2J_e+1} \sqrt{2F_e+1} \sqrt{2F_g+1} \begin{pmatrix} F_e & 1 & F_g \\ -m_e & q & m_g \end{pmatrix} \begin{Bmatrix} F_e & 1 & F_g \\ J_g & I & J_e \end{Bmatrix}, \quad (7)$$

the parenthesis and curly brackets denote, respectively, the $3j$ and $6j$ symbols, g and e point respectively ground and excited states.

Formulas (1-7) have been used to calculate frequency shift and modification of intensity for corresponding transitions (for more details see [12]). The frequency shifts of atomic transitions 2, 5, 8, 3, 6 and 9 versus magnetic B -field in respect to initial position (the corresponding initial positions at $B = 0$ are indicated by the arrows) are presented by solid curves in Fig. 6. The black squares are the experimental results, i.e. frequency shifts of VSOPs labeled 2, 5, 8, 3, 6 and 9 (numbers denote the corresponding transitions, see Fig. 2). As it is seen the theoretical model very well describes the observed results. In Fig. 6 are shown only the atomic transitions (represented by VSOPs) which are observed in the spectra (particularly, atomic transition $F_g = 1 \rightarrow F_e = 0$ is omitted). It is interesting to note, that the frequency of the transition labeled 8 remains practically the same in the range of 100 – 1100 G, while g -factors for the ground and excited levels are -0.7 MHz/G and 0.93 MHz/G respectively. Thus, in the linear Zeeman effect (i.e. when

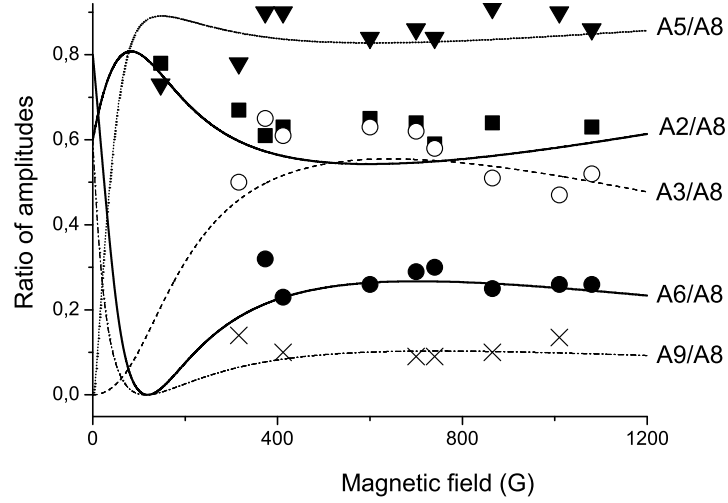


Fig. 7. The ratio of the amplitudes (i.e. ratio of the probabilities) A_i/A_8 ($i = 2, 3, 5, 6, 9$) in the case of π -excitation versus magnetic B -field: experimental points are presented by squares, hollow circles, triangles, filled circles, and crosses, correspondingly and theory by solid, dashed, dotted, solid, and dot-dashed lines, correspondingly. It is easy to visually track behavior of the forbidden transitions 3 and 5 since at $B = 0$ the probabilities are zero.

a frequency shift is proportional to B -field) one expects to detect a shift of ~ 1600 MHz when $B = 1000$ G, while the shift is nearly zero. Obviously, this is caused by the influence of the neighboring levels with the selection rules presented by formula (2). Another interesting point is that for transition labeled 6 there is deviation from the linear Zeeman for small field values of order of a few Gauss. Note, that atomic transition represented by VSOP labeled 2 can be a convenient one for an external magnetic field measurement since it has constant frequency shift of 1.28 MHz/G in the whole region 1 – 1000 G. Also, the probability of this atomic transition is high enough and this is displayed by the large amplitude of VSOP labeled 2. The transition labeled 9 indicates a higher constant frequency shift than transition 2, but (see Fig. 5) intensity of transition 9 (displayed by small amplitude of VSOP labeled 9) is essentially lower.

Let's now consider the change in the probability of atomic transition versus applied magnetic B -field. As it was demonstrated in [10,11,12] the change in the probability (i.e. change of the dipole moment) causes the change in the Rabi frequency of the laser radiation and, as a consequence, the change in the efficiency of optical pumping process. This is displayed as an increase or decrease in the corresponding VSOP resonance amplitude presented on the spectra at Figs. (3-5). Note, that in the experiment it is more convenient to measure the ratio of the VSOPs amplitudes, A_2 , A_3 , A_5 , A_6 , A_8 and A_9 of the corresponding transitions as a function of B , since the absolute value of the VSOP

amplitude depends on the laser intensity, scanning time of an atomic transition by a frequency of laser radiation, nano-cell temperature, *etc.* Consequently in Fig. 7 shown are experimental (squares, hollow circles, triangles, filled circles, and crosses, correspondingly) and theoretical (by solid, dashed, dotted, solid, and dot-dashed cuves, correspondingly) ratios of the A_2 , A_3 , A_5 , A_6 , A_9 divided by A_8 (A_8 is chosen since the amplitude of VSOP denoted 8 changes most slowly among the others). Note, that coincidence of the experiment and the theory is not as good as it is for the frequency shift. The explanation is as follows: since the VSOP is located exactly at the atomic transitions, thus a shift of the VSOP frequency displays exactly the shift of the atomic transition. As to the VSOP amplitude, although, it linearly depends on the probability of corresponding atomic transition, however some other factors can also have a slight influence. However, if we consider VSOP resonances formed by the widely used SA technique, they are not useful for the above mentioned study since the ratio of the amplitudes of VSOP resonances completely doesn't match the ratio of the corresponding transition probabilities.

4 Conclusion

By experimental exploration of the λ -Zeeman technique based on Rb nano-cell use, we reveal for the first time (both experimentally and theoretically) a strong modification of atomic transitions probabilities versus magnetic B -field in the range of 100 – 1100 G, of the ^{87}Rb , D_2 line $F_g = 1 \rightarrow F_e = 0, 1, 2, 3$ transitions, including $F_g = 1, m_F = 0 \rightarrow F_e = 1, m_F = 0$ and $F_g = 1, m_F = -1 \rightarrow F_e = 3, m_F = -1$ transitions (these transitions are "forbidden" when $B = 0$). Note, that these two forbidden transitions at $B > 150$ G are among the strongest atomic transitions in the detected spectra.

It is shown that the observed frequency shifts of the $F_g = 1 \rightarrow F_e = 0, 1, 2, 3$ atomic transitions in an external magnetic field $B > 150$ G are very well described by the developed theoretical model. Particularly, $F_g = 1, m_F = +1 \rightarrow F_e = 1, m_F = +1$ atomic transition is a unique one since its frequency remains practically unchanged when B varies in the range of 100 – 1100 G (this is evidence of another type of non-linear Zeeman shift). For an external magnetic field measurement the $F_g = 1, m_F = -1 \rightarrow F_e = 2, m_F = -1$ atomic transition can be a convenient one, since it has a constant frequency shift of 1.28 MHz/G in the whole region of 1 – 1000 G. Also, the probability of this atomic transition is high enough and this is displayed by the large amplitude of the corresponding VSOP resonance.

The experimental results are in a good agreement with the theoretical calculations. It is worth to note, that the presented experimental results obtained with the help of Rb nano-cell (i.e. λ -Zeeman technique) might be obtained using expensive and complicated systems based either on cold and trapped atoms or collimated several-meter long Rb atomic beam propagating in vacuum conditions.

Simple and robust λ -Zeeman technique can be successfully implemented also for the study of the D_1 and D_2 lines of Na, K, Cs and other atoms.

5 Acknowledgement

The authors are grateful to A. Sarkisyan for his valuable participation in fabrication of the NTC as well as to A. Papoyan, A. Sargsyan and A. Bagdasaryan for useful discussions. Research conducted in the scope of the International Associated Laboratory (CNRS-France & SCS-Armenia) IRMAS.

References

1. D. Budker, D. F. Kimball, and D. P. DeMille, *Atomic Physics* (Oxford Univ. Press, Oxford, 2004).
2. D. Meschede, *Optics, Light and Lasers: The practical Approach to Modern Aspects of Photonics and Laser Physics* (Second Edition WILEY-VCH Verlag GmbH&Co. KGaA, Weinheim, 2004)
3. P. Tremblay, A. Michaud, M. Levesque, S. Theriault, M. Breton, J. Beaubien and N. Cyr, Phys. Rev. A **42**, (1990) 2766-2773.
4. N. Papageorgiou, A. Weis, V. Sautenkov, D. Bloch and M. Ducloy, Appl. Phys. B **59**, (1994) 123-126.
5. M. U. Momeen, G. Rangarajan and P. C. Deshmukh, J. Phys. B: At. Mol. Opt. Phys. **40**, (2007) 3163-3172.
6. G. Školnik, N. Vujicic, T. Ban, Opt. Commun., **282**, (2009) 1326.
7. D. Sarkisyan, A. Papoyan, T. Varzhapetyan, K. Blush and M. Auzinsh, J. Opt. Soc. Am. B **22**, (2005) 88-95.
8. D. Sarkisyan, A. Papoyan, T. Varzhapetyan, J. Alnis, K. Blush and M. Auzinsh, J. Opt. A: Pure and Appl. Opt. **6**, (2004) S142-S150.
9. G. Hakhumyan, D. Sarkisyan, A. Sargsyan, A. Atvars, and M. Auzinsh, Optics and Spectroscopy, **108**, (2010) 685-692.
10. T. S. Varzhapetyan, G. T. Hakhumyan, V. V. Babushkin, D. H. Sarkisyan, A. Atvars and M. Auzinsh, J. of Contemp. Phys. (Arm. Acad. of Sci.) **42**, (2007) 223-229.
11. A. Sargsyan, G. Hakhumyan, A. Papoyan, D. Sarkisyan, A. Atvars and M. Auzinsh, Appl. Phys. Lett. **93**, (2008) 021119.
12. G. Hakhumyan, C. Leroy, Y. Pashayan-Leroy, D. Sarkisyan, M. Auzinsh, Opt. Commun., **284**, (2011) 4007-4012.
13. D. Sarkisyan, A. Papoyan, *Optical processes in micro- and nanometric thin cells containing atomic vapor*, *New Trends in Quantum Coherence and Nonlinear Optics* (Horizons in World Physics, Nova Science Publishers, 2009).
14. D. Sarkisyan, D. Bloch, A. Papoyan and M. Ducloy, Opt. Commun. **200**, (2001) 201-208.
15. W. Demtroder, *Laser Spectroscopy: Basic Concepts and Instrumentation* (Springer, 2002).
16. M. Auzinsh, D. Budker, S. M. Rochester, *Optically Polarized Atoms: Understanding Light-Atom Interactions*, (Oxford University Press, 2011).